Electronic Supplementary Information (ESI) for Energy & Environmental Science.

Supporting Information

Manipulating Zn 002 deposition plane with zirconium ion crosslinked hydrogel electrolyte toward dendrite free Zn metal anodes

Yong Cheng, Yucong Jiao* and Peiyi Wu*

Department State Key Laboratory for Modification of Chemical Fibers and Polymer Materials, College of Chemistry and Chemical Engineering, Donghua University, Shanghai 201620, China.

E-mail: wupeiyi@dhu.edu.cn; yucong.jiao@dhu.edu.cn

Content

Experimental Procedures

Materials

Acrylamide (AM) monomer and poly(ethylene glycol) diacrylate (PEGDA, Mn~575) were procured from Sigma-Aldrich Co., Ltd. Zinc perchlorate hexahydrate ($Zn(ClO_4)_2 \cdot 6H_2O$), zirconium oxychloride octahydrate ($ZrOCl_2 \cdot 8H_2O$) and aniline monomer were sourced from Aladdin Co., Ltd. Silk fibroin (SF) was purchased from XinTianSi Co., Ltd. (Huzhou, China). Zinc foil was obtained from Qingyuan Metal Co., Ltd. The carbon cloth was supplied by Ce-Tech Co., Ltd.

Preparation of SFPAM-Zr hydrogel electrolyte

A mixture of 10 wt.% SF solution and 4.8 g AM monomer was firstly prepared with vigorously stirring. Subsequently, I2959 (0.1 wt.% for AM monomer) and PEGDA-575 (0.1 wt.% for monomer) were added to the mixture following with polymerized under UV light for 40 min to obtain SFPAM hydrogel. The SFPAM-Zr hydrogel electrolyte was achieved by immersing SFPAM hydrogel in an electrolyte solution containing 2 M $Zn(ClO_4)_2$ and 0.01 M $ZrOCl_2$ for 12 h. The SFPAM hydrogel electrolyte was prepared by soaking SFPAM hydrogel in 2 M $Zn(ClO_4)_2$ solution for 12 h.

Preparation of PANI/CC cathode

The PANI/CC cathode was synthesized via a typical in situ polymerization method[1]. Generally, the aniline monomer is polymerized on carbon cloth in an ice bath with 1 M HCl solution. The product was then washed and vacuum dried to obtain the PANI/CC cathode.

Materials characterization

The mechanical strength of the hydrogel electrolyte was evaluated by the testing machine of UTM2103 (Shenzhen Suns Technology Co., Ltd.). The morphologies and components of the hydrogel electrolyte were examined with scanning electron microscopy (SEM, Hitachi SU8230) and energy-dispersive X-ray spectroscopy (EDS). Fourier transform infrared spectrometer (FTIR, Nicolet iS50) and X-ray photoelectron spectroscopy (XPS, Escalab 250Xi) were employed to characterize the interactions in SFPAM-Zr. The crystal plane and surface morphology of Zn metal were detected by means of Powder X-ray diffractometer (XRD, D/max-2550VB) and scanning electron microscopy (SEM, Hitachi SU8230).

Electrochemical measurements

The ionic conductivity determined by electrochemical impedance spectroscopy (EIS, CHI760E) was calculated with the following equation (1):

$$\sigma = \frac{l}{R*S} \qquad \text{Equation (1)}$$

Where l is the electrolyte thickness, S denotes the area, and R signifies the resistance.

The transference number of Zn^{2+} was performed on Autolab electrochemical workstation (M204) and calculated according to equation (2)[2]:

$$t_{Zn^{2+}} = \frac{R_{cell}}{R_{DC}} \qquad \text{Equation (2)}$$

Where R_{cell} represents the resistance prior to polarization, RDC is obtained by the applied potential of 20 mV and the steady-state current.

The Tafel and HER test were both conducted by the three-electrode system, with the saturated calomel electrode (SCE), platinum plate and Zn plate as reference, counter, and working electrode, respectively. The Chronoamperometry (CA) was conducted with an overpotential of -150 mV. The zeta potential was collected on Zeta potential analyzer (SurPASS 3, Andon paar). The electric double layer capacitance was examined in a voltage range of -0.015-0.015 V, with scaning rates from 4 mV s^{-1} to 10 mV s^{-1}. The in situ electrochemical impedance spectroscopy (EIS) was implemented for symmetrical Zn battery with 3 minutes deposition and 3 minutes rest at 1 mA cm^{-2}. The galvanostatic intermittent titration technique (GITT) tests were performed with a discharge pulse of 40 s at 0.5 A g^{-1}, and a rest period of 1800 s. The cyclic voltammetry (CV) of Zn/PANI cell was recorded in the range between 0.5 V and 1.5 V on an Autolab electrochemical workstation. The shelving-recovery charge/discharge performance was tested under the current density of 8 mA cm^{-2}, and shelving for 20 h after every 80 cycles.

Density functional theory (DFT) calculations

DFT calculations were carried out using the Vienna ab-initio Simulation Package (VASP) with the projector-augmented wave (PAW) method. All calculations were based on the same generalized gradient approximation (GGA) method with Perdew-Burke-Ernzerhof (PBE) functional for the exchange-correlation term. Van der Waals interaction was taken into account at DFT-D3 with Becke-Jonson damping level. An energy cutoff of 500 eV and Gamma-centered 3 × 3 × 1 k-points mesh were applied to absorption calculations. The convergence thresholds for energy were set as 10^{-6} eV during ion relaxation, and the convergence thresholds for force was set as 0.02 eV·$Å^{-1}$. Visualization of the structures is made by using VESTA software. Ea was calculated by the energy difference of the system after and before adsorption:

$$Ea = E_{A\text{-}substrate} - E_A - E_{substrate}$$

where $E_{A\text{-}substrate}$, E_A, and $E_{substrate}$ represent the energies of the A adsorbed surface, A atom or molecule, and the surface, respectively.

To model Zn or Zr diffusion on Zn(002) surface, the climbing-image nudged elastic band (CI-NEB) method with 4 images was applied and each transition state was confirmed to have a single imaginary

vibrational frequency along the reaction coordinate. The convergence thresholds for energy were set as 10^{-6} eV and the convergence thresholds for force were set as 0.05 eV·Å^{-1} in CI-NEB procedure.

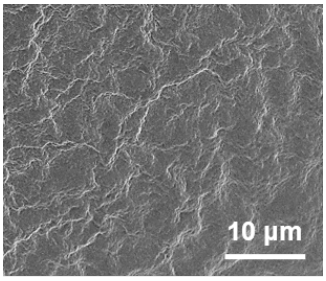

Fig. S1 The SEM image for surface morphology of SFPAM-Zr hydrogel electrolyte.

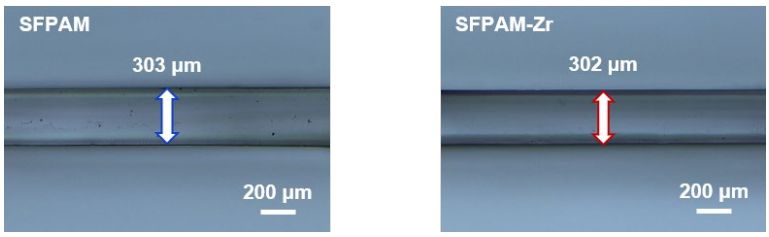

Fig. S2 Optical microscope images of SFPAM and SFPAM-Zr.

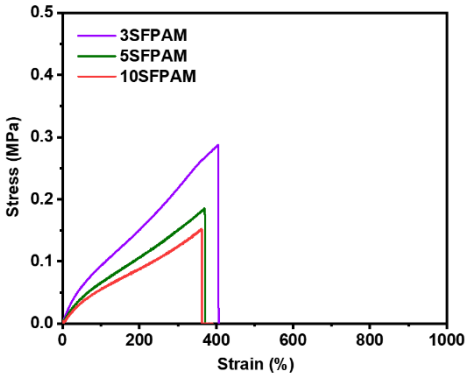

Fig. S3 The tensile stress-strain curves for SFPAM-Zr hydrogel electrolyte with different silk fibroin weight ratios.

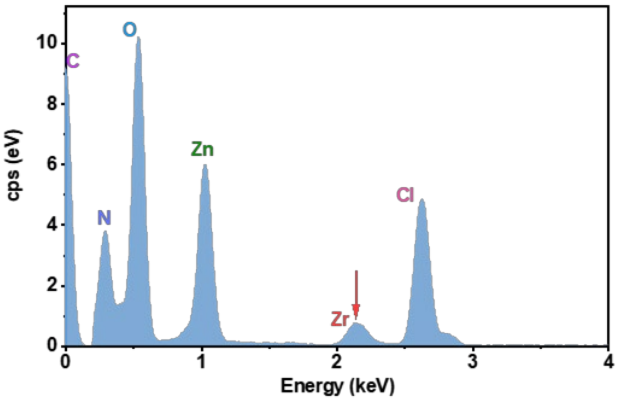

Fig. S4 EDS data for SFPAM-Zr hydrogel electrolyte.

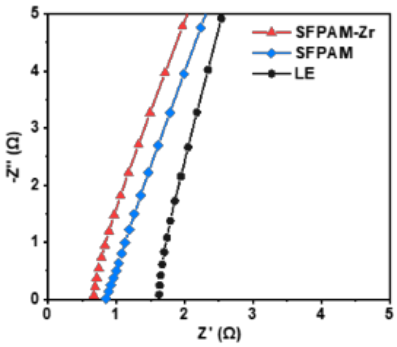

Fig. S5 AC impedance spectra for SFPAM-Zr, SFPAM and LE.

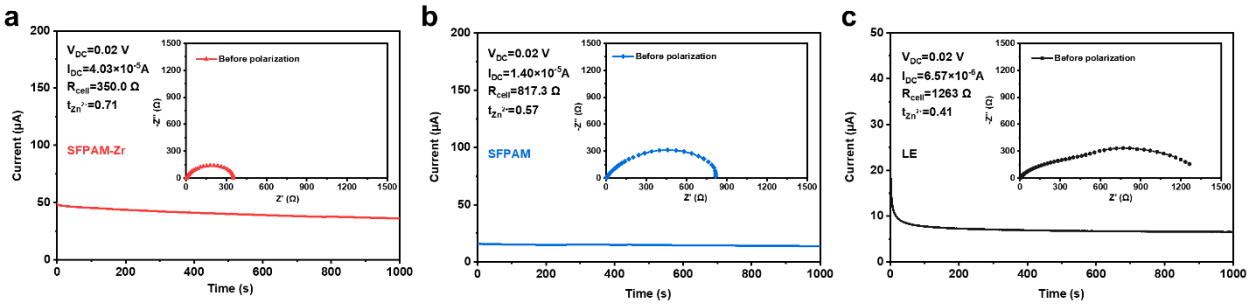

Fig. S6 Zn^{2+} transference number characterizations for (a) SFPAM-Zr, (b) SFPAM, and (c) LE.

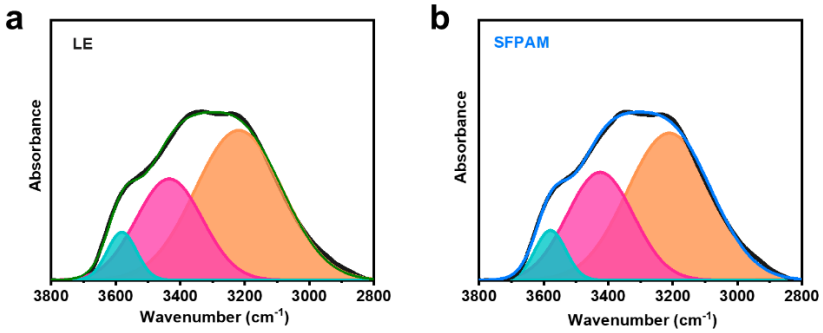

Fig. S7 The fitted FTIR spectra for LE and SFPAM in the range between 3800-2800 cm^{-1}.

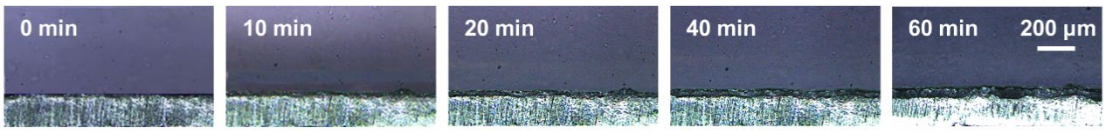

Fig. S8 *In situ* optical images of Zn plating behaviors with SFPAM electrolyte.

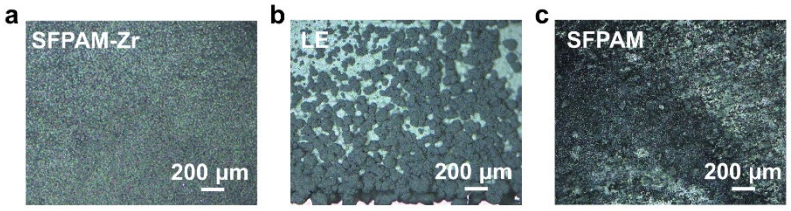

Fig. S9 Optical images of Zn metal surface after plating at the current density of 10 mA cm^{-2} with (a) SFPAM-Zr (b) LE and (c) SFPAM for 60 min.

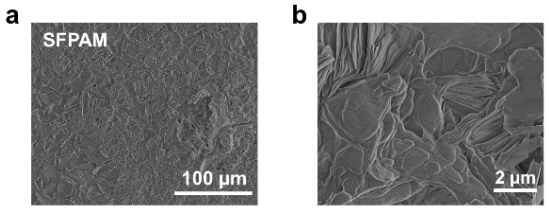

Fig. S10 SEM images of the Zn metal surface after plating for 60 min with SFPAM.

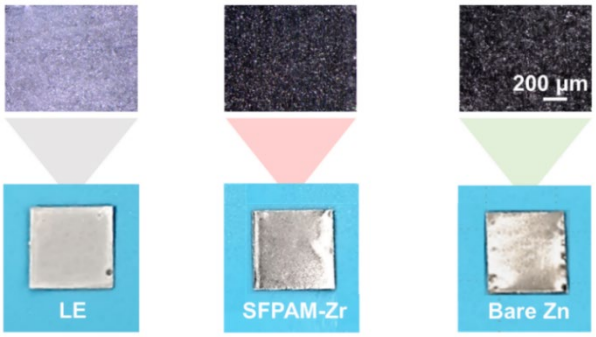

Fig. S11 Optical images of the Zn metal surface before and after covering with SFPAM-Zr and immersing in LE for 9 h.

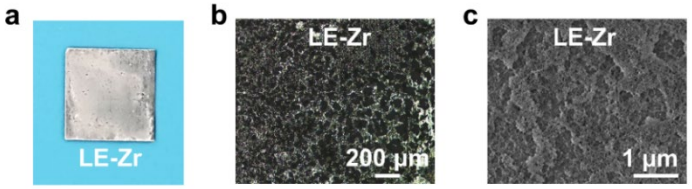

Fig. S12 The (a, b) optical and (c) SEM images of the Zn metal surface after immersing in LE-Zr electrolyte for 12 h.

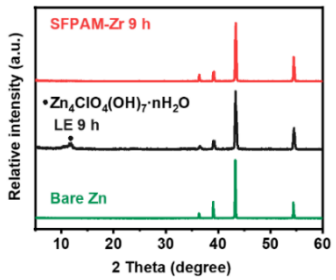

Fig. S13 XRD patterns of the Zn metal covered with SFPAM-Zr and immersed in LE for 9 h, respectively.

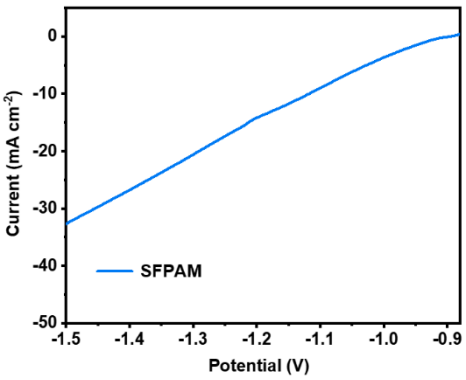

Fig. S14 The HER curve for Zn metal with SFPAM.

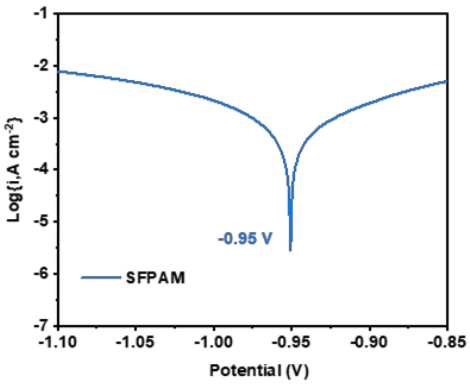

Fig. S15 The Tafel curve for Zn metal with SFPAM.

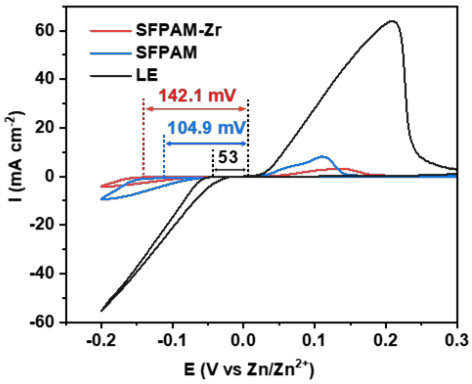

Fig. S16 Cyclic voltammetry curves for Zn metal with SFPAM-Zr, LE and SFPAM, respectively.

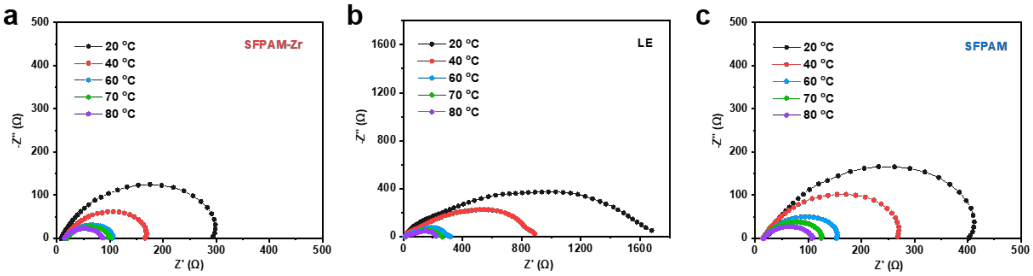

Fig. S17 EIS characterizations for the symmetrical Zn batteries with (a) SFPAM-Zr, (b) LE, and (c) SFPAM.

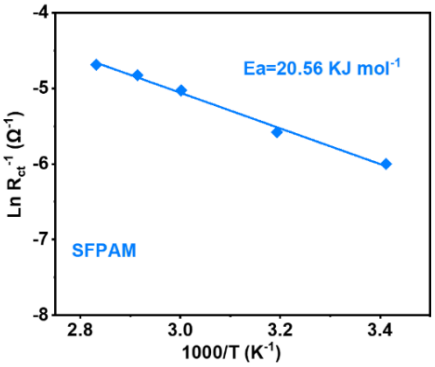

Fig. S18 The calculated Ea result for symmetrical Zn battery with SFPAM.

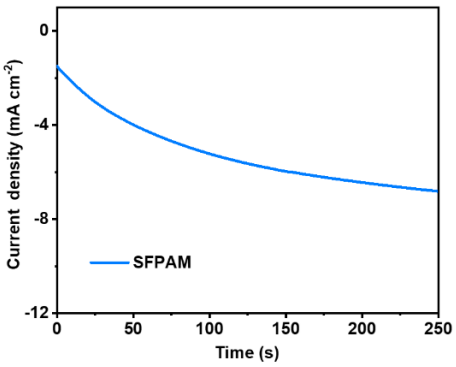

Fig. S19 The CA curve for symmetrical Zn battery with SFPAM.

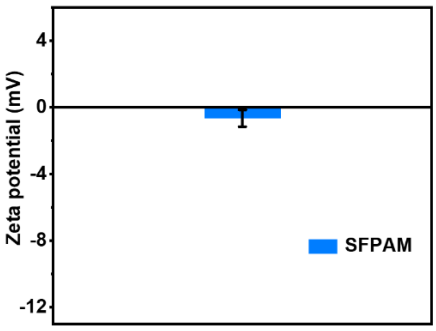

Fig. S20 The Zeta potential of Zn metal after deposited with SFPAM.

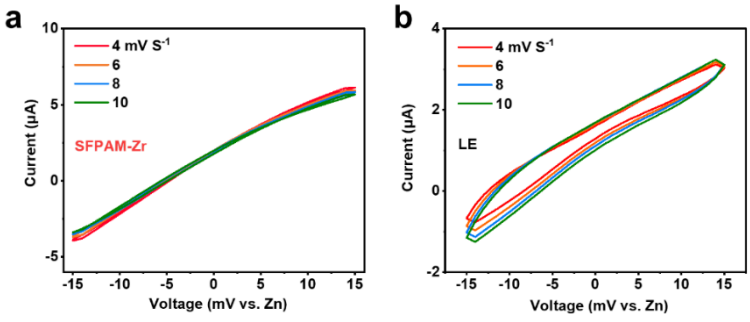

Fig. S21 CV profiles of the symmetrical Zn battery with (a) SFPAM-Zr and (b) LE.

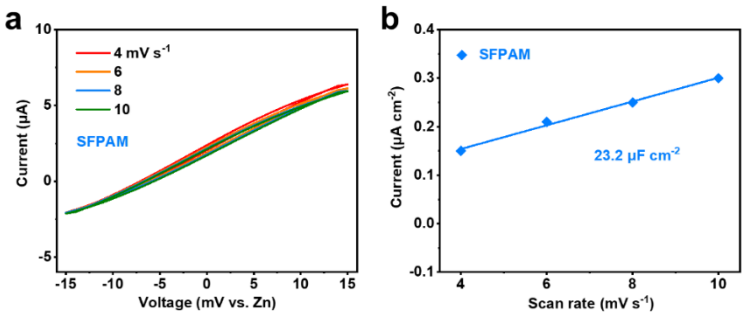

Fig. S22 (a) CV profiles of the symmetrical Zn battery with SFPAM. (b) EDL measurements for Zn metal with SFPAM.

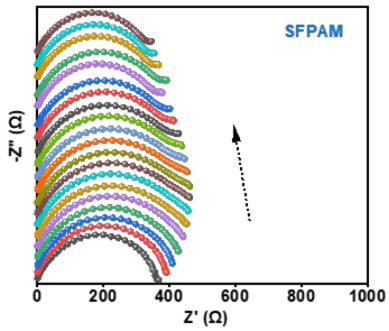

Fig. S23 *In situ* EIS curves for symmetrical Zn battery with SFPAM.

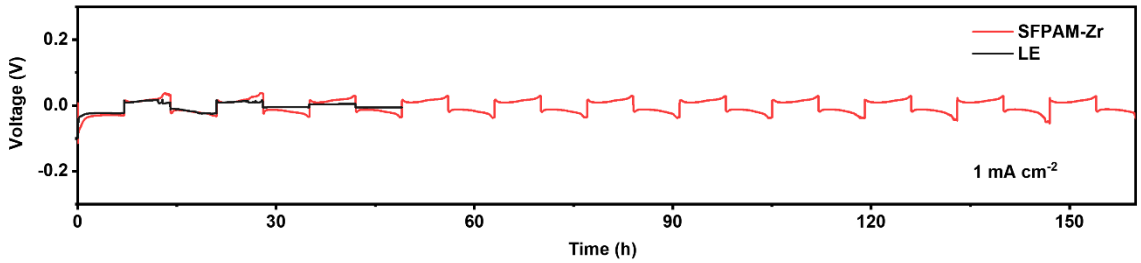

Fig. S24 The stripping/plating performance of symmetrical Zn cell with SFPAM-Zr and LE at 1 mA cm^{-2} and 7 mA h cm^{-2}.

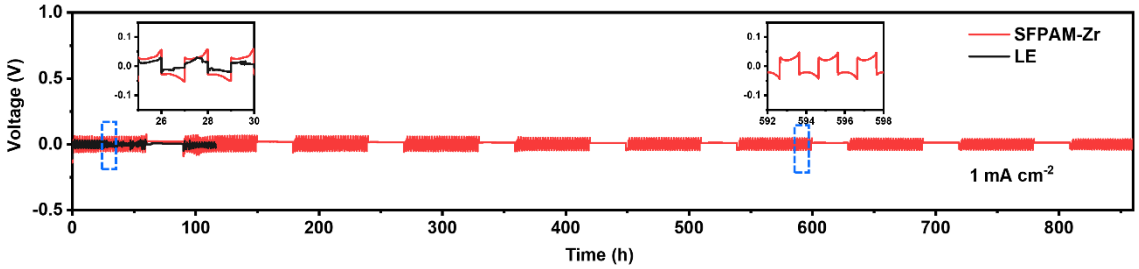

Fig. S25 Shelving-recovery performance of SFPAM-Zr and LE at 1mA cm^{-2} and 1 mA h cm^{-2}.

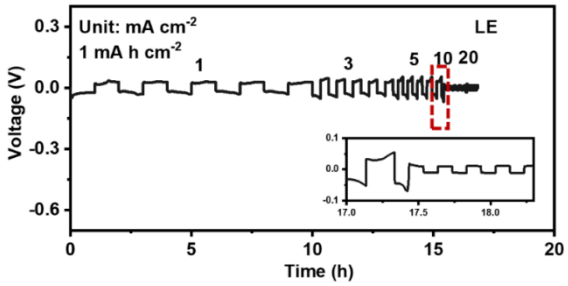

Fig. S26 The rate performance of symmetrical Zn cell with LE.

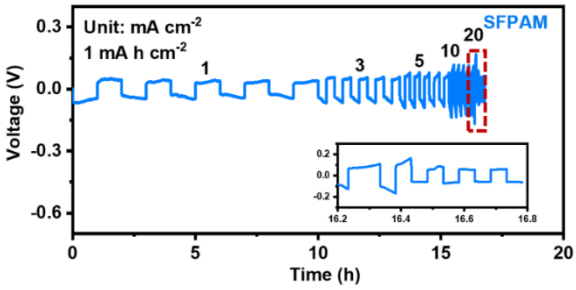

Fig. S27 The rate performance of symmetrical Zn cell with SFPAM.

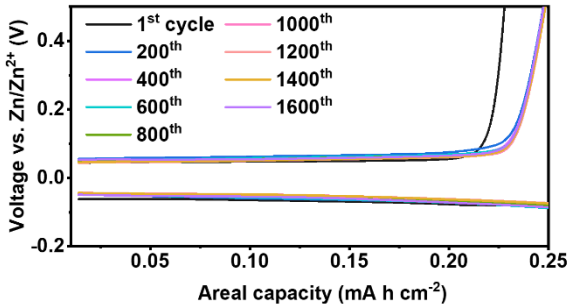

Fig. S28 The voltage/capacity curves for asymmetrical Zn/Cu cell with SFPAM-Zr at different cycles.

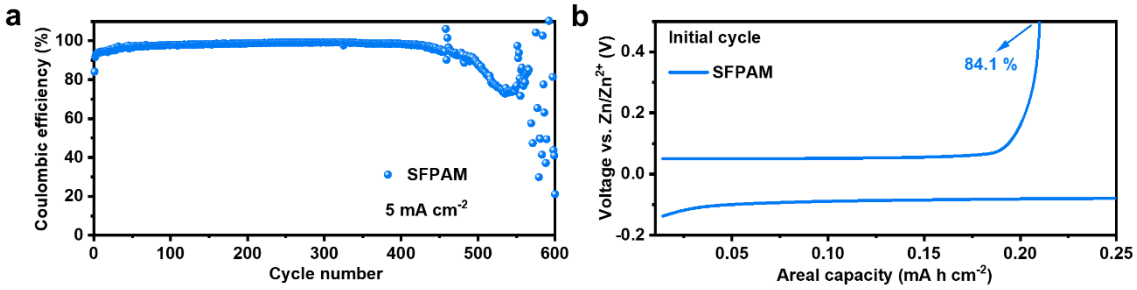

Fig. S29 (a) The CE performance of the asymmetrical Zn/Cu battery with SFPAM at current density of 5 mA cm^{-2}, and (b) the corresponding initial cycle curves.

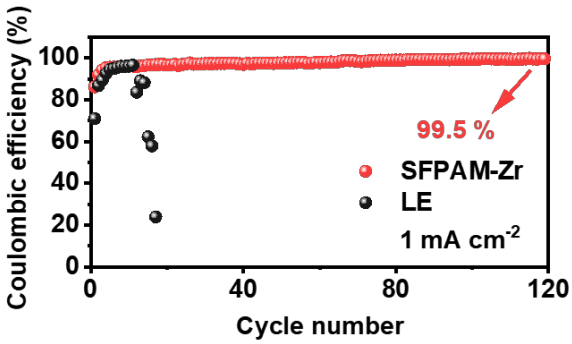

Fig. S30 The CE performance of the asymmetrical Zn/Cu cell with SFPAM-Zr and LE at 1 mA cm^{-2} for 1 mA h cm^{-2}.

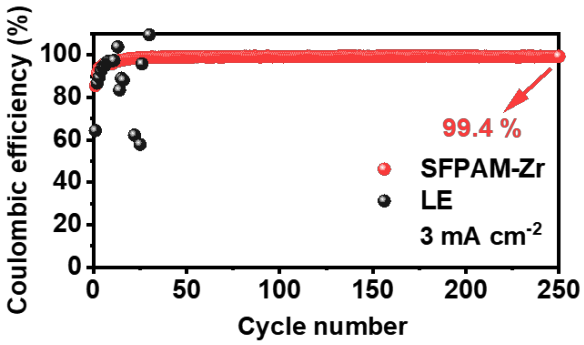

Fig. S31 The CE performance of the asymmetrical Zn/Cu cell with SFPAM-Zr and LE at 3 mA cm^{-2} for 1 mA h cm^{-2}.

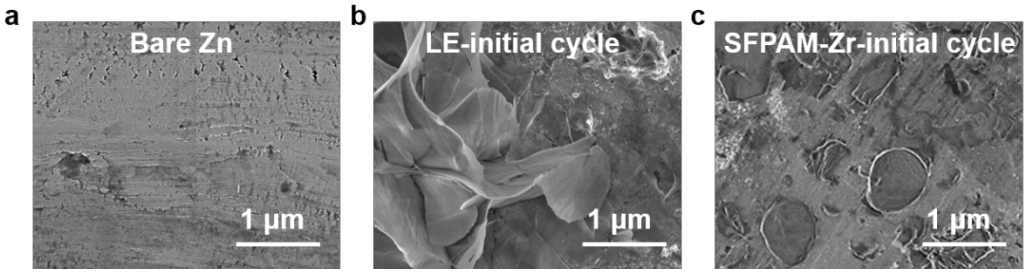

Fig. S32 The SEM images of (a) bare Zn, Zn metal after the initial cycle with (b) LE and (c) SFPAM-Zr.

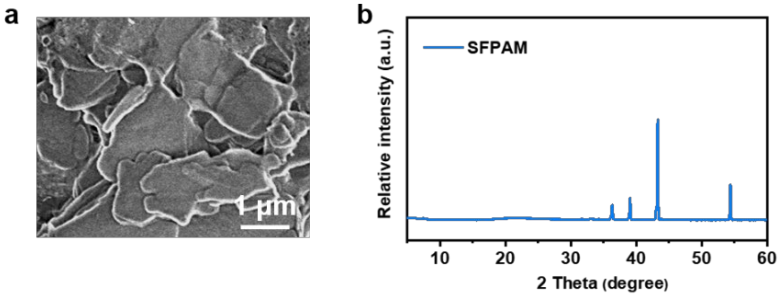

Fig. S33 The (a) SEM image and (b) XRD pattern for the Zn metal of symmetrical Zn battery with SFPAM after 10 cycles.

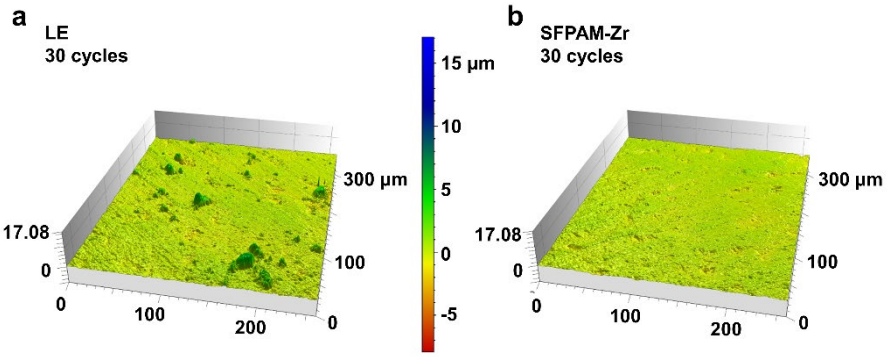

Fig. S34 CLMS images of Zn metal after 30 cycles with (a) LE and (b) SFPAM-Zr.

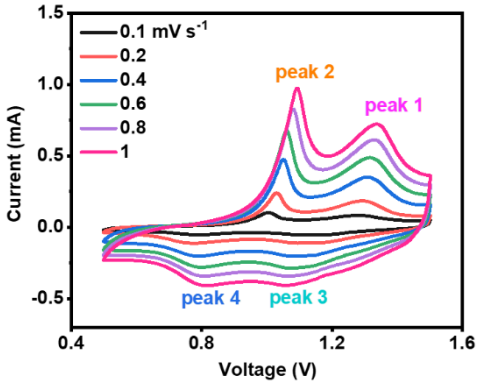

Fig. S35 CV curves of the Zn/PANI battery with SFPAM-Zr at different scan rate from 0.1 to 1 mV s^{-1}.

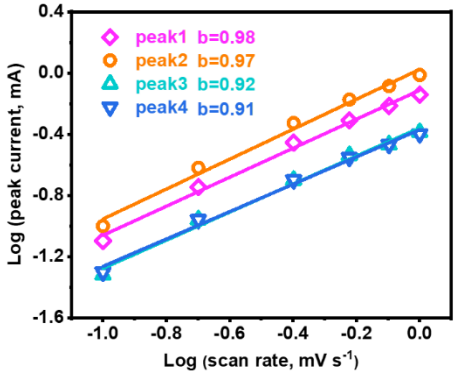

Fig. S36 The plots for log (peak current) versus log (scan rate).

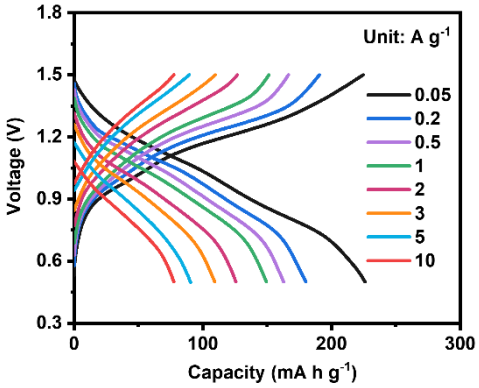

Fig. S37 The discharge/charge curves for the Zn/PANI battery with SFPAM-Zr at different current densities.

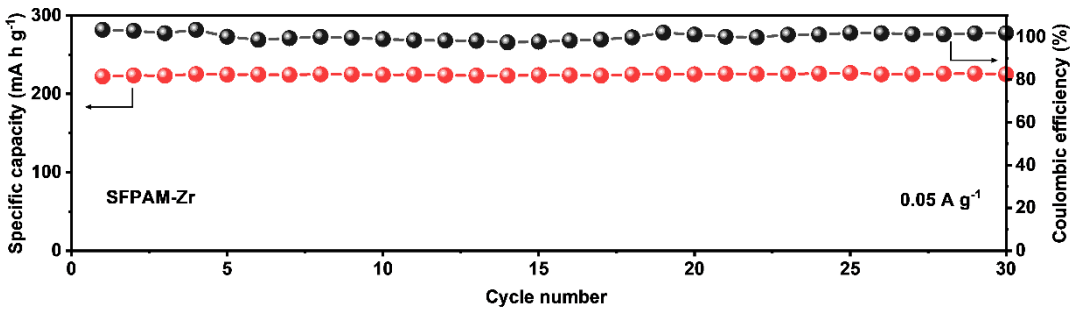

Fig. S38 Cycling performance of the Zn/PANI battery with SFPAM-Zr at 0.05 A g^{-1}.

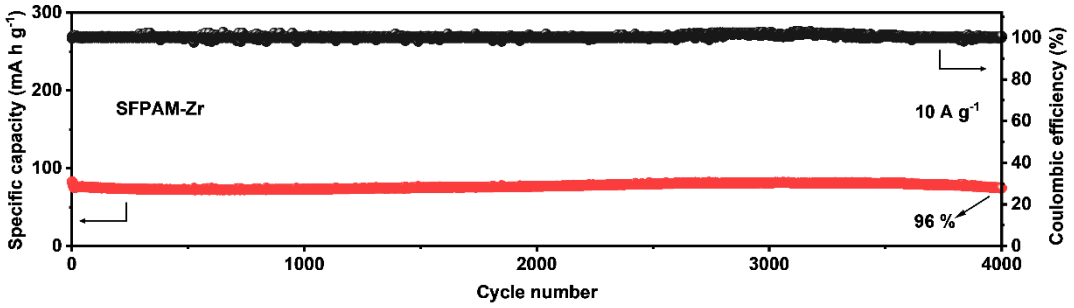

Fig. S39 Cycling performance of the Zn/PANI battery with SFPAM-Zr at 10 A g^{-1}.

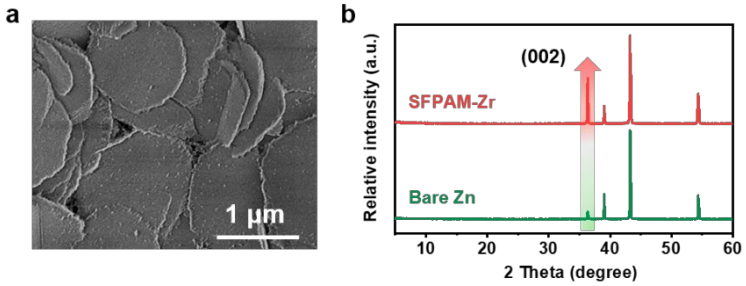

Fig. S40 The (a) SEM image and (b) XRD patterns of Zn metal anode after 2500 cycles with SFPAM-Zr for Zn/PANI battery.

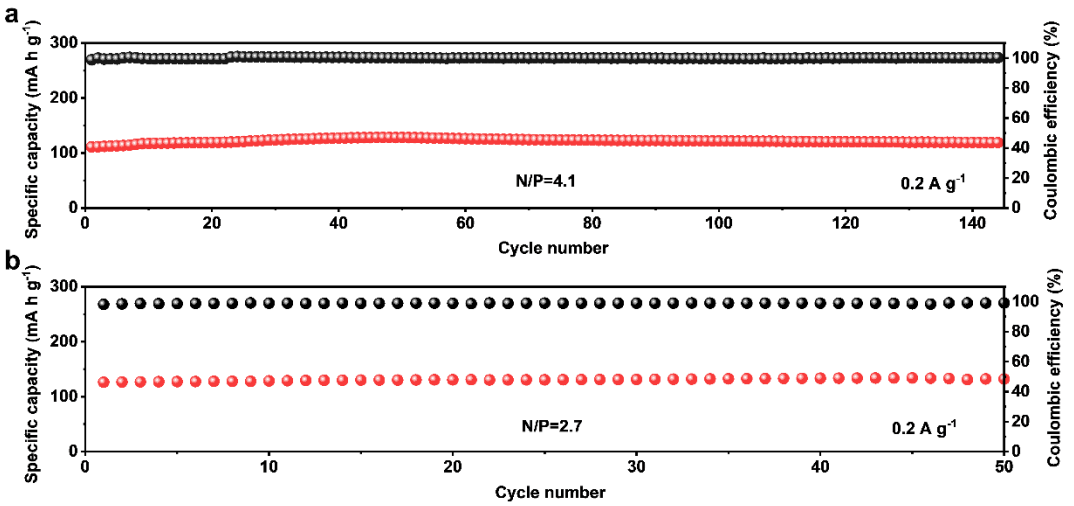

Fig. S41 The cycling performance of the Zn/PANI batteries with SFPAM-Zr at the N/P ratio of (a) 4.1 and (b) 2.7.

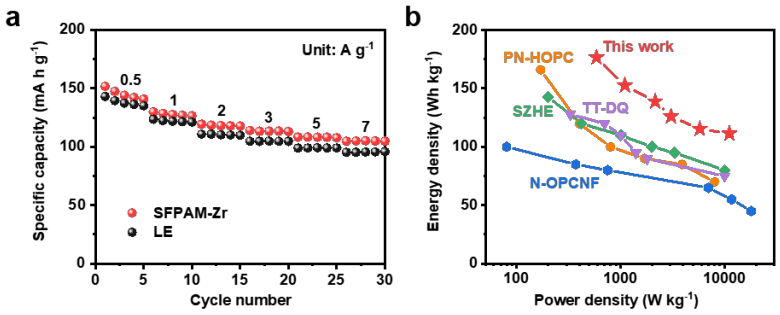

Fig. S42 (a) The rate performance of Zn/AC capacitors with SFPAM-Zr and LE at different current densities. (b) Ragone plots of Zn/AC capacitor with SFPAM-Zr and recently reported works.[3-6]

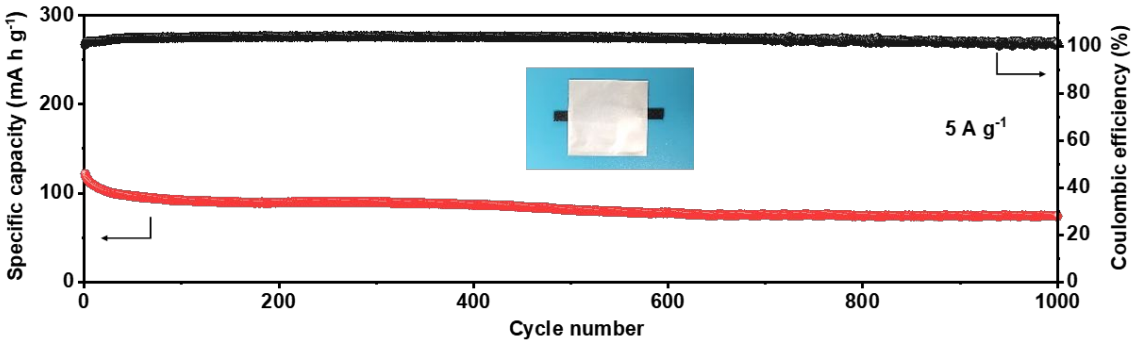

Fig. S43 Cycling performance of the flexible Zn/PANI with SFPAM-Zr at 5 A g^{-1}.

Supplementary Table

Table S1. Comparisons of the N/P ratio between this work and other reported Zn batteries.

Modified strategies	Cathode	Zn anode	Current density	Areal capacity (mA h cm^{-2})	N/P ratio	Reference
SFPAM-Zr gel	**PANI**	**10 μm Zn**	**0.2 A g^{-1}**	**1.8**	**2.7**	**This work**
SFPAM-Zr gel	**PANI**	**20 μm Zn**	**0.2 A g^{-1}**	**1.9**	**4.1**	**This work**
Gelatin coating	V_6O_{13}	50 μm Zn	0.1 A g^{-1}	0.75	35.06	7
PVB coating	MnO_2	10 μm Zn	1C	0.28	16.86	8
DX/$ZnSO_4$	$NH_4V_4O_{10}$	20 μm Zn	2 A g^{-1}	2	8	9
PEGDA additive	ZnVO	10 μm Zn	5 A g^{-1}	~ 0.52	6.4	10
FCOF coating	MnO_2	~ 20 μm Zn	4 mA cm^{-2}	~ 1.44	5	11
TMU20	$NH_4V_4O_{10}$	10 μm Zn	0.5 A g^{-1}	~ 1.2	4.01	12
RME	$Zn_{0.25}V_2O_5$•nH_2O	30 μm Zn	56 mA g^{-1}	5.5	3.2	13
BE-ZrP	LMO	Zn powder	1C	1.1	3	14

References

1 F. Wan, L. Zhang, X. Wang, S. Bi, Z. Niu, J. Chen, *Adv. Funct. Mater*., 2018, **28**, 1804975.

2 K. Leng, G. Li, J. Guo, X. Zhang, A. Wang, X. Liu, J. Luo, *Adv. Funct. Mater*., 2020, **30**, 2001317.

3 Z. Peng, A. G. Bannov, S. Li, Y. Huang, L. Tang, L. Tan, Y. Chen, *Adv. Funct. Mater*., 2023, **33**, 2303205.

4 H. He, J. Lian, C. Chen, Q. Xiong, C. Li, M. Zhang, *Nano-Micro Lett*., 2022, **14**, 106.

5 Q. Fu, S. Hao, X. Zhang, H. Zhao, F. Xu, J. Yang, *Energy Environ. Sci*., 2023, **16**, 1291-1311.

6 L. Wang, M. Peng, J. Chen, T. Hu, K. Yuan, Y. Chen, *Adv. Mater*., 2022, **34**, 2203744.

7 J. Shin, J. Lee, Y. Kim, Y. Park, M. Kim and J. W. Choi, *Adv. Energy Mater*., 2021, **11**, 2100676.

8 J. Hao, X. Li, S. Zhang, F. Yang, X. Zeng, S. Zhang, G. Bo, C. Wang and Z. Guo, *Adv. Funct. Mater*., 2020, **30**, 2001263.

9 T. Wei, Y. Ren, Y. Wang, L. Mo, Z. Li, H. Zhang, L. Hu and G. Cao, *ACS Nano*., 2023, **17**, 3765-3775.

10 J. Zhao, C. Song, S. Ma, Q. Gao, Z. Li, Y. Dai and G. Li, *Energy Storage Mater*., 2023, **61**, 102880.

11 Z. Zhao, R. Wang, C. Peng, W. Chen, T. Wu, B. Hu, W. Weng, Y. Yao, J. Zeng, Z. Chen, P. Liu, Y. Liu, G. Li, J. Guo, H. Lu and Z. Guo, *Nat. Commun*., 2021, **12**, 6606.

12 Z. Li, Y. Liao, Y. Wang, J. Cong, H. Ji, Z. Huang and Y. Huang, *Energy Storage Mater*., 2023, **56**, 174-182.

13 Y. Wang, T. Wang, S. Bu, J. Zhu, Y. Wang, R. Zhang, H. Hong, W. Zhang, J. Fan and C. Zhi, *Nat. Commun*., 2023, **14**, 1828.

14 H. Peng, C. Wang, D. Wang, X. Song, C. Zhang and J. Yang, *Angew. Chem. Int. Ed*., 2023, **62**, e202308068.